Fast initial guess estimation for digital image correlation

Peihan Tu[a,*]
[a]Guangdong University of Technology, School of Automation, Waihuanxi Road, Guangzhou, China, 510006

Abstract. Digital image correlation (DIC) is a widely used optical metrology for quantitative deformation measurement due to its non-contact, low-cost, highly precise feature. DIC relies on nonlinear optimization algorithm. Thus it is quite important to efficiently obtain a reliable initial guess. The most widely used method for obtaining initial guess is reliability-guided digital image correlation (RG-DIC) method, which is reliable but path-dependent. This path-dependent method limits the further improvement of computation speed of DIC using parallel computing technology, and error of calculation may be spread out along the calculation path. Therefore, a reliable and path-independent algorithm which is able to provide reliable initial guess is desirable to reach full potential of the ability of parallel computing. In this paper, an algorithm used for initial guess estimation is proposed. Numerical and real experiments show that the proposed algorithm, adaptive incremental dissimilarity approximations algorithm (A-IDA), has the following characteristics: 1) Compared with inverse compositional Gauss-Newton (IC-GN) sub-pixel registration algorithm, the computational time required by A-IDA algorithm is negligible, especially when subset size is relatively large; 2) the efficiency of A-IDA algorithm is less influenced by search range; 3) the efficiency is less influenced by subset size; 4) it is easy to select the threshold for the proposed algorithm.

Keywords: digital image correlation, fast algorithm, computer vision, deformation measurement.

***First Author, E-mail: peihan.tu@outlook.com

1. Introduction

Digital image correlation (DIC) is a convenient, non-contact and low-cost tool for full-field deformation measurement [1]. During the past several years, significant progresses have been made in terms of the accuracy, robustness and efficiency of DIC.

In the aspect of accuracy, several sub-pixel registration algorithms have been developed, including the correlation coefficient curve-fitting method (CCCFM) [2], the gradient-based method (GBM) [3, 4], and the classic Newton-Raphson algorithm [5, 6] with forward additive mapping strategy (FA-NR). CCCFM and GBM algorithm are fast but not considered the influence of strain. Though FA-NR algorithm gives a better performance in terms of the accuracy of DIC, the computation cost is expensive. The problem became increasingly critical with the rapid increment of the number of the point of interest (POI). Recently, it is a trend to develop adaptive

DIC algorithm. By optimize either the selection of subset size or sampling locations in subsets, researchers obtain more accurate and precise displacement and strain fields [7, 8]. Moreover, principles from p-adaptive finite element analysis are introduced to obtain a self-adapting higher order mesh in the finite-element-based global DIC algorithms [9]. These methods, though improve the accuracy of DIC, are computed more expensively due to the introduction of new parameters. The reduction of computation complexity is desirable for the real-time DIC.

In view of robustness, it is improved in some specific situations, which greatly expands the usage of DIC. To measure a large deformation, Pan et al developed a novel approach to ensure the rapid and correct convergence of the nonlinear optimization algorithm by providing an accurate and reliable initial guess [10]. Poissant proposed a "sutset splitting" procedure for discontinuous displacement fields, for example, a crack [11]. Valle et al. proposed the Heaviside-based DIC method for the study of materials including multiple crossing cracks [12]. To circumvent the problem resulted from light reflections, DIC algorithm based on single minimization with several pairs of images where the reflections are located in different regions is proposed [13]. To decrease the influence of change in light condition, a weighted normalized gradient-based algorithm [14] is proposed due to the insensitivity of the gradient to the illumination variation.

At the same time, inverse compositional Gauss-Newton (IC-GN) algorithm has been introduced to increase the efficiency of DIC. The main benefit of IC-GN over FA-NR is its computation efficiency advantage by eliminating repeated calculation of intensity gradients and the inverse of the Hessian matrix during the iterations [15]. Recently, with the rapid development of parallel computing technology, GPU-based DIC algorithms have also been noticed by researchers. However, DIC algorithm based on reliability-guided displacement tracking (RGDT) strategy is reliable but path-dependent [19], which limits the further improvement of computation

speed of DIC using parallel computing technology, and error of calculation may be spread out along the calculation path. To reduce these negative influences, Pan proposed an improved RGDT strategy using a two-section tracking scheme [16] to give play to the ability of parallel computing. Jiang et al. developed a path-independent fast Fourier transform-based cross correlation (FFT-CC) algorithm to estimate the initial guess [17, 18], while it is sensitive to small deformation and only applied to rectangular subset. Wu et al proposed an efficient integer-pixel search scheme with combination of an improved particle swarm optimization (PSO) algorithm and the block-based gradient descent search (BBGDS) algorithm [20], but it cannot guarantee the optimum because the search may be trapped in a local region. A reliable and path-independent algorithm which is able to provide reliable initial guess is desirable to reach full potential of the ability of parallel computing.

In this paper, a template matching algorithm called incremental dissimilarity approximations (IDA) is introduced into DIC, which overcomes the deficiencies of FFT-CC algorithm and the algorithm adopting PSO and BBGDS. IDA is proposed in 2009 by Tombari for fast template matching [21]. It prunes most subset candidates using a threshold with little addition/subtraction operations, which reduce the computation complexity. The original IDA is based on sum absolute difference (SAD) or sum square difference (SSD) criteria. Though SAD and SSD are efficient to calculate, they are influenced by speckle pattern, subset size and image noise, thus the threshold required by IDA is also influenced by these factors. For simpler setup of the threshold, adaptive scheme with modified SAD is applied in improved IDA algorithm. The numerical and real experiments show that the initial guess obtained by adaptive IDA (A-IDA) algorithm is able to make IC-GN algorithm converge fast without sacrifice of accuracy.

This paper is organized as follows: section 2 gives a brief introduction of DIC; in section 3, the principles of A-IDA algorithm are presented; section 4 examines the feasibility and effectiveness of the proposed algorithm; section 5 concludes our work.

2. Basic Principle of DIC

In traditional DIC, a square subset located at the center of an interested point (x_0, y_0) is selected as reference subset $f(x, y)$ with a size of $N \times N$ pixels (N is an odd number) in the reference image. Then DIC algorithms find the target subset $g(x', y')$ in the target image. Using first-order warp function, the relationship between (x, y) and (x', y') is given as

$$\begin{aligned} x' &= x_0 + \Delta x + u + u_x \Delta x + u_y \Delta y, \\ y' &= y_0 + \Delta y + v + v_x \Delta x + v_y \Delta y. \end{aligned} \tag{1}$$

Where u and v are the displacement components of the interested point (x_0, y_0) in x-axis and y-axis; u_x, u_y, v_x and v_y represent their gradient components; Δx and Δy are the distances between (x_0, y_0) and (x, y) in x-axis and y-axis, respectively.

To obtain the target subset with speed, accuracy and robustness, the standard displacement tracking algorithm in path-independent DIC [18, 20] can be simply described as a two-step procedure:

a) Obtain initial guess using integer-pixel registration.

In this step, the following zero-normalized cross-correlation (ZNCC) criterion is often used:

$$C_{ZNCC} = \frac{\sum_{x,y} [f(x,y) - f_m] \cdot [g(x',y') - g_m]}{\sqrt{\sum_{x,y} [f(x,y) - f_m]^2 \sum_{x,y} [g(x,y) - g_m]^2}}. \tag{2}$$

b) Optimize displacement parameters using nonlinear optimization methods, such as FA-NR and IC-GN algorithms. IC-GN is more efficient than FA-NR and with approximately equivalent accuracy. For IC-GN algorithm, the following zero-normalized sum of squared differences (ZNSSD) criterion is used:

$$C_{ZNSSD} = \sum_{x,y}\left[\frac{f(x,y)-f_m}{\sqrt{\sum_{x,y}[f(x,y)-f_m]^2}} - \frac{g(x',y')-g_m}{\sqrt{\sum_{x,y}[g(x',y')-g_m]^2}}\right]^2, \quad (3)$$

where $f_m = \frac{1}{N^2}\sum_{x,y} f(x,y)$, $g_m = \frac{1}{N^2}\sum_{x,y} g(x',y')$.

3. Theory

3.1. Standard IDA algorithm

For simplicity, given a vector *A* of length *k* as target image, *S* is a one-dimensional reference subset with a length of *r*. As *S* slides on *A*, there are $k - r + 1$ candidate target vectors *C* (one-dimensional target subset). For reference subset *S* and each candidates *C*, they are correspondingly divided into *p* sub-vectors [21]: s_i, c_i, $i = 1,\ldots p$ (it is not necessary for *p* sub-vectors to contain the same number of components).

Partial sum absolute difference (PSAD) is defined as

$$\mathrm{PSAD}(i) = \sum_{j=1}^{\mathrm{num}(s_i \text{ or } c_i)} \left| s_{i,\,j} - c_{i,\,j} \right|. \quad (4)$$

Partial one-norm (PON) is defined as

$$\mathrm{PON}(S,i) = \sum_{j=1}^{\mathrm{num}(s_i \text{ or } c_i)} \left| s_{i,\,j} \right|, \mathrm{PON}(C,i) = \sum_{j=1}^{\mathrm{num}(s_i \text{ or } c_i)} \left| c_{i,\,j} \right|, \quad (5)$$

where num(•) represents the number of components in s_i (c_i). $s_{i,\,j}$ ($c_{i,\,j}$) represents the j^{th} component in s_i (c_i).

Then, the following inequality is established by using triangular inequality principal

$$\mathrm{PSAD}(i) \geq \left|\mathrm{PON}(S,i) - \mathrm{PON}(C,i)\right| \quad i = 1,\ldots p. \quad (6)$$

In addition,

$$\mathrm{SAD} = \sum_{i=1}^{p} \mathrm{PSAD}(i) \geq \sum_{i=1}^{p} \left|\mathrm{PON}(S,i) - \mathrm{PON}(C,i)\right|. \quad (7)$$

According to Eq. (6) and (7), a threshold *th* can be set to discriminate the matching and nonmatching candidates for the dissimilarity criterion SAD.

$$\sum_{i=1}^{p}\left|\mathrm{PON}(S,i)-\mathrm{PON}(C,i)\right|>th\,. \tag{8}$$

If Eq. (8) does not hold, which means *C* is not a nonmatching candidate, a tighter lower bound can be obtained by replacing the left term of Eq. (8) by the use of triangular inequality principal.

$$\mathrm{PSAD}(t)+\sum_{i=1,i\neq t}^{p}\left|\mathrm{PON}(S,i)-\mathrm{PON}(C,i)\right|>th \quad t\in\{1,...p\}, \tag{9}$$

In fact, this process is repeated until SAD between *S* and *C* is calculated or a pruning condition based on a tighter lower bound is satisfied.

$$\begin{aligned}&\mathrm{SAD}=\sum_{i=1}^{p}\mathrm{PSAD}(i)\geq...\geq\mathrm{PSAD}(q)+\mathrm{PSAD}(t)+\sum_{i=1,i\neq t,i\neq q}^{p}\left|\mathrm{PON}(S,i)-\mathrm{PON}(C,i)\right|\geq\\&\mathrm{PASD}(t)+\sum_{i=1,i\neq t}^{p}\left|\mathrm{PON}(S,i)-\mathrm{PON}(C,i)\right| \qquad (10)\\&\geq\sum_{i=1}^{p}\left|\mathrm{PON}(S,i)-\mathrm{PON}(C,i)\right|>th\end{aligned}$$

Finally,

$$\mathrm{SAD}=\sum_{i=1}^{p}\mathrm{PSAD}(i)>th\,, \tag{11}$$

If Eq. (11) does not hold, then *C* is a matching candidate. The target subset can be obtained from the set of matching candidates by selecting the candidate with minimum SAD.

It seems to be unclear why this algorithm can improve the speed of template matching (integer-pixel registration). The reasons are that

a) PON can be pre-computed quickly and independently using fast incremental calculation schemes [22], while PSAD (thus SAD) cannot;

b) A large number of calculations are spared if candidates are pruned by Eq. (8). In fact, Eq. (8) prunes most of nonmatching candidates if a proper threshold is selected.

c) The tighter the lower bound is, computationally the more demanding function is calculated.

For two-dimensional rectangular subset, *S* and *C* are partitioned into *p* equally sized rectangular regions along the rows. It should be noted that irregular subset can also be used in IDA

algorithms by partitioning it into p irregular parts. In this work, only rectangular subset is considered.

3.2. Adaptive IDA (A-IDA) algorithms

According to section 3.1, the threshold is very critical because it determines whether the algorithm can succeed in obtaining the target subset with integer-pixel accuracy. When threshold is small, IDA algorithm will probably fail without obtaining target subset. When threshold is large, the efficiency reduces and sometimes is even lower than simple integer-pixel searching. First of all, to overcome these deficiencies, the single values *th* is modified to a simple equation $th \cdot \sqrt{\sum_{k \in S} \left(S_k - \bar{S}\right)^2}$, where $\bar{S}$ represents the average of *S*. Combined with this modification, a new A-IDA algorithm is proposed by adjusting the value *th* adaptively.

The detailed descriptions of A-IDA algorithm are as follows.

Step 1: Standard IDA algorithm with modified threshold th_0 is used to discriminate all the candidates. A series of sets A_1, A_2, A_3, … A_{p+1} are created by collecting the candidates which are pruned by different inequalities in Eq. (10) (the right term of these inequities is "*th*"). There are $p + 1$ sets which corresponds to $p + 1$ inequalities. For example, if the left term of an inequality is $PASD(q) + PASD(t) + \sum_{i=1, i \neq t, i \neq q}^{p} \left| PON(S,i) - PON(C,i) \right|$, then a candidate pruned by this inequality belongs to A_3.

Step 2: Check whether the top (with the biggest subscript) nonempty set A_{TN} is A_{p+1}. If not, then that's mean the matching candidates are not obtained and the algorithm proceeds to step 3. Otherwise, pick the candidate with minimum SAD which belongs to A_{TN} (A_{p+1}) as target image with integer-pixel accuracy.

Step 3: Let $th \leftarrow th + d_{th}$ and repeat step 1 which now discriminates the candidates within A_{TN}. d_{th}, which is equal to 1, is the increment of adaptive threshold in A-IDA algorithm.

From the description of the A-IDA algorithm, it is evident that initial threshold th_0 is easier to be determined due to the introduction of adaptive scheme (Step 3). Moreover, the modified threshold is less influenced by subset size but highly influenced by speckle patterns and image noises. Therefore, pre-processed speckle images are used in the process of integer-pixel registration. The speckle images are blurred using normalized box filter [22], and then the histograms of the speckle images are equalized [23]. Image blurring is able to reduce the influence of image noise on the threshold. Histogram equalization (HE) can reduce the influence of the variation of speckle patterns on it and increase the difference between reference subset and nonmatching candidate. With the help of the two pre-processed methods, the setup of threshold of A-IDA is relatively fixed in the application of DIC. Fig. 1 presents a flow chart that describes the procedures of the proposed A-IDA algorithm, where the lower subscript q, which is to the right of "Eq. (10)", indicates q^{th} inequality (from the right) in Eq. (10).

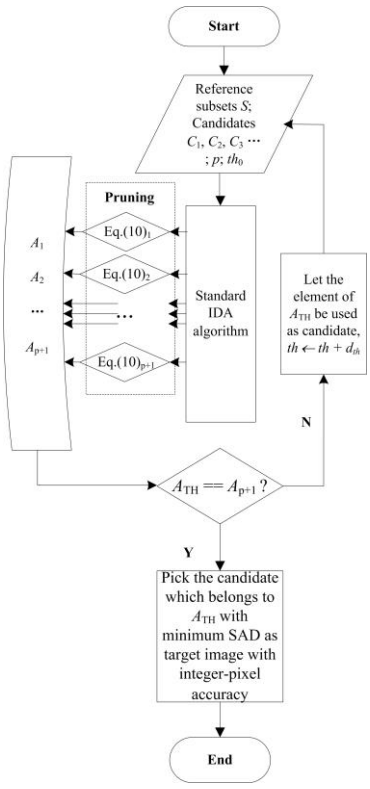

Fig. 1 The flow chart of the newly proposed A-IDA algorithm

3.3. Inverse Compositional Gauss-Newton Algorithm

Compared with FA-NR algorithm, IC-GN is more efficient to compute mainly due to its avoidance of repeatedly calculating Hessian matrix. The principle is briefly introduced in this section. More details can be found in [15].

Consider the ZNSSD criterion with an affine warp function

$$C_{ZNSSD} = \sum_{\xi} \left\{ \frac{f(\mathbf{x} + \mathbf{W}(\xi;\Delta\mathbf{p})) - \bar{f}}{\Delta f} - \frac{g(\mathbf{x} + \mathbf{W}(\xi;\mathbf{p})) - \bar{g}}{\Delta g} \right\}^2, \tag{12}$$

$$\mathbf{W}(\xi;\mathbf{p}) = \begin{bmatrix} 1+u_x & u_y & u \\ v_x & 1+v_y & v \\ 0 & 0 & 1 \end{bmatrix} \begin{bmatrix} \Delta x \\ \Delta y \\ 1 \end{bmatrix}. \tag{13}$$

Where $f(x)$, $g(x)$ denotes the gray level at global pixel coordinates x; $\bar{f}$, $\bar{g}$ represent the average of reference and target subsets; $\xi = [\Delta x, \Delta y, 1]^T$ is the local coordinates in reference or target

subsets; $\Delta f = \sqrt{\left[f(\mathbf{x}+\mathbf{W}(\xi;\Delta\mathbf{p}))-\bar{f}\right]^2}$ and $\Delta g = \sqrt{\left[g(\mathbf{x}+\mathbf{W}(\xi;\mathbf{p}))-\bar{g}\right]^2}$; $\mathbf{p} = [u, u_x, u_y, v, v_x, v_y]^{\mathrm{T}}$ and its increment $\Delta\mathrm{p} = [\Delta u, \Delta u_x, \Delta u_y, \Delta v, \Delta v_x, \Delta v_y]^{\mathrm{T}}$.

Eq. (12) is a least-square problem, which can be solved from Eq. (14) by minimizing C_{ZNSSD} with respect to $\Delta\mathrm{p}$

$$\Delta\mathbf{p} = -\mathbf{H}^{-1}_{6\times6} \times \sum_{\xi}\left(\nabla f \frac{\partial \mathbf{W}}{\partial \mathbf{p}}\right)^{T}_{6\times1} \cdot \left[f(\mathbf{x}+\xi) - \bar{f} - \frac{\Delta f}{\Delta g}\left(g(\mathbf{x}+\mathbf{W}(\xi;\mathbf{p}))-\bar{g}\right)\right]. \tag{14}$$

Different from FA-NR algorithm, the warp function of the target subset is updated in the following way

$$\mathbf{W}(\xi;\mathbf{p}) \leftarrow \mathbf{W}(\xi;\mathbf{p}) \circ \mathbf{W}^{-1}(\xi;\Delta\mathbf{p}). \tag{15}$$

The iteration calculation is repeated until convergence conditions $\|\Delta\mathbf{p}\| \le 0.001$ are satisfied.

IC-GN algorithm is approved as an efficient method for sub-pixel registration in DIC. Compared with FA-NR, IC-GN is more suitable to implement in the real-time DIC, due to its constant parameters in the iteration calculation, for example, Hessian matrix. Particularly, Pan et al. [15] used interpolation coefficient look-up table for bicubic interpolation, which further reduce the redundant computation in IC-GN algorithm. These pre-computations, at the beginning of IC-GN algorithm, make IC-GN algorithm more efficient and keep the same accuracy as that of FA-NR.

4. Experimental Verification

To demonstrate the performance of the proposed algorithm, numerical and real experiments are conducted in the aspects of speed and accuracy. The proposed method was coded using C++ language and run on a laptop computer (Inter(R) Core (TM) i7-4510U CPU with main frequency 2.00GHz, 4GB RAM).

4.1. Numerical experiment

As shown in Fig. 2, 8bit speckle images with a size of 300 × 300 pixels are numerically generated, which contain 3000 speckles with a radius of 3 pixels. Gaussian noise with mean 0, variance 4 is added into these speckle images. The speckle images used in A-IDA algorithm are pre-processed using box filter [22] with blurring kernel size 15 × 15 pixels and histogram equalization [23]. It should be noted that the time of preprocessing is negligible compared with those of A-IDA and IC-GN algorithms, thus the data is not given in the paper. A region of interest (ROI) centered at (150, 150) of the reference image is of size 200 × 200 pixels. There are 101 × 101 = 10201 interested points regularly distributed in the ROI. The grid step is 2 pixels. Rigid body translation is applied to the reference images, varying from 0 to 21. The step is 1.05 pixels. The subset size ranged between 21 × 21 and 63 × 63 pixels are investigated in the numerical experiments and the step is 6 pixels. In the process of integer-pixel registration, the search range in x-axis is [-5, +5] pixels. The search range in y-axis varies from [-5, 15] to [-5, 45] pixels. The initial threshold th0 is also investigated in the numerical experiments, which varies from 0.5 to 6 and the step is 0.5. In the process of IC-GN algorithm, the subset is of the same size as that used in A-IDA algorithm, and the convergence conditions of the algorithms are set be the norm of the incremental displacement vector being equal to or less than 10^{-4} pixels. In the numerical experiments, the basic parameters are: 33 × 33 pixels subset, th_0 = 1, search range in y-axis [-5, 45] and 10.50 pre-set displacement. The others parameters are unchanged when one of these variables is investigated in the experiments.

Fig. 3 shows the mean bias error and standard deviation [15] of the rigid body translation experiments. Tables 1–4 show the average computational time at each POI with respect to pre-set displacement, search range, subset size and initial threshold, respectively. From these tables, it can

be concluded: 1) the computational time consumed by A-IDA is about one-sixth of that by IC-GN algorithm (Table 1); 2) the average computational time is less influenced by search range; the experiments show the growth of computational time is slower than linear growth with respect to search range (Table 2); as the search range in y-axis is [-5, +15], the average computational time at each POI is 0.06 ms; as the search range in y-axis is [-5, +45], it is 0.10ms; 3) the efficiency is less influenced by subset size; as subset size increases from 21 to 63 (Table 3), the average computational time at each POI increases from 0.11 to 0.15 ms; hence, it is evident that the computational time required by A-IDA algorithm will become negligible compared with that by IC-GN algorithm with the increment of subset size; 4) it is easy to select the initial threshold (Table 4); the variation of computational time is smaller than 0.1 ms as the threshold th_0 increases from 0.5 to 6.0; the selection of the threshold has less influence on the efficiency.

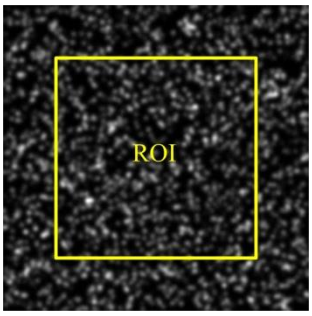

Fig. 2 Reference image and ROI

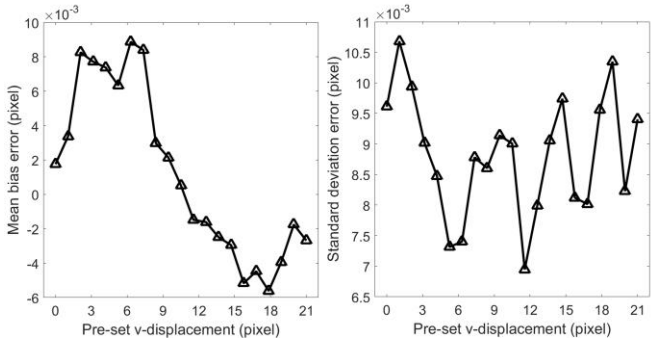

Fig. 3 Mean bias and standard deviation error of rigid body translation experiments; subset size 33, th_0 = 1, search range in y-axis [-5, 45]

Table 1 Average computational time at each POI with respect to pre-set displacement using A-IDA and IC-GN algorithm; subset size 33 × 33 pixels, th_0 = 1, search range in y-axis [-5, 45]

Pre-set displacement (pixel)	Average computational time (ms)	
	A-IDA	IC-GN
1.05	0.10	0.55
2.10	0.10	0.57
3.15	0.10	0.57
4.20	0.10	0.60
5.25	0.11	0.61
6.30	0.10	0.62
7.35	0.10	0.62
8.40	0.10	0.65
9.45	0.10	0.65
10.50	0.10	0.64
11.55	0.10	0.63
12.60	0.10	0.63
13.65	0.10	0.62
14.70	0.10	0.62
15.75	0.10	0.63
16.80	0.11	0.61
17.85	0.10	0.60
18.90	0.10	0.57
19.95	0.10	0.55
21.00	0.10	0.54

Table 2 Average computational time at each POI with respect to search range; pre-set displacement 10.50 pixels, subset size 33 × 33 pixels, th_0 = 1

search range in y-axis (pixel)	Average computational time (ms)
[-5, 15]	0.06
[-5, 25]	0.07
[-5, 35]	0.08
[-5, 45]	0.10

Table 3 Average computational time at each POI with respect to subset size; pre-set displacement 10.50 pixels, th_0 = 1, search range in y-axis [-5, 45]

Subset size (pixel)	Average computational time (ms)
21	0.11
27	0.12
33	0.11
39	0.12
45	0.12
51	0.14
57	0.14
63	0.15

Table 4 Average computational time at each POI with respect to initial threshold; pre-set displacement 10.50 pixels, subset size 33 × 33 pixels, search range in y-axis [-5, 45]

threshold th_0	Average computational time (ms)
0.5	0.17
1.0	0.10
1.5	0.11
2.0	0.11
2.5	0.11
3.0	0.13
3.5	0.13
4.0	0.16
4.5	0.16
5.0	0.18
5.5	0.20
6.0	0.21

4.2. Experiment using real data

The reference and target images are downloaded from DIC challenge datasets [24]. A ROI with a size of 200 × 200 pixels is located at (800, 200) of the reference image, as shown in Fig. 4.

There are 101 × 101 POIs regularly distributed in each reference image with a grid step 2 pixels. The subset size is 33 × 33 pixels with p = 3. The search ranges are [-20, +20] and [-5, +5] in x-axis and y-axis, respectively. The speckle images used in A-IDA algorithm are pre-processed using box filter [22] with a blurring kernel size of 15 × 15 pixels and histogram equalization technique [23]. The initial threshold th0, which varies from 0.5 to 6, is investigated in the real experiments. Fig. 5 shows the displacement fields u and v in x-axis and y-axis. Table 5 shows the average computational time with respect to th_0 at each POI consumed by A-IDA and IC-GN algorithm. The efficiencies of A-IDA in numerical and real experiments are almost at the same level, but the computational time of IC-GN in real experiments is slower than that in numerical experiments. That's because the shape change of the subset which makes IC-GN algorithm require more iterations to satisfy the convergent condition. Moreover, although the speckle images are very different from those generated in numerical experiments, the influence of th_0 in real experiments on efficiency is approximately the same as that in numerical experiments.

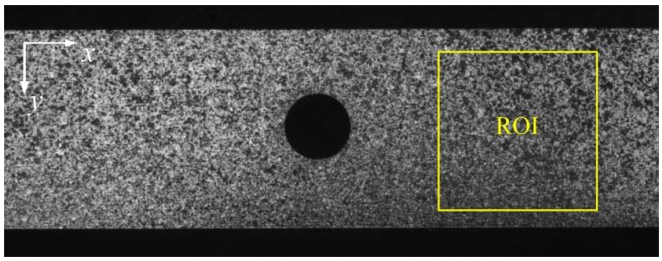

Fig. 4 Reference image and the ROI

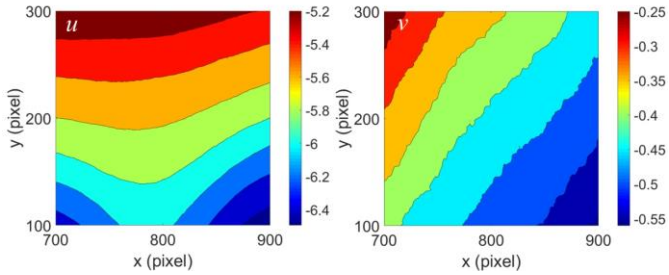

Fig. 5 Displacement fields in x-axis and y-axis

Table 5 Average computational time with respect to th_0 at each POI using A-IDA and IC-GN algorithm in the real experiments; subset size is 33 × 33 pixels with p = 3 and the search ranges are [-20, +20] and [-5, +5] in x-axis and y-axis, respectively

th_0	Average computational time (ms)	
	A-IDA	IC-GN
0.5	0.16	0.81
1.0	0.11	0.83
1.5	0.11	0.83
2.0	0.12	0.81
2.5	0.11	0.80
3.0	0.13	0.80
3.5	0.13	0.80
4.0	0.16	0.81
4.5	0.17	0.83
5.0	0.19	0.81
5.5	0.19	0.81
6.0	0.20	0.82

5. Discussion and Conclusion

It should be noted that p also influences the performance of the proposed algorithm. In most cases, the A-IDA algorithm is more efficient if a higher p is used with bigger templates [21]. In practical use, the p ranged between 3 and 8 is recommended. In addition, all the subset sizes are

divisible by $p = 3$ in this paper. In fact, divisibility is not mandatory. Intuitively, however, the most efficient way is to divide the subset into several equally sized rectangular regions.

In this paper, an initial guess estimation algorithm, A-IDA, is proposed for DIC. The proposed algorithm has the following characteristics: 1) Compared with IC-GN algorithm, the computational time required by A-IDA algorithm is negligible, especially when subset size is relatively large; 2) the efficiency of A-IDA algorithm is less influenced by search range; the experiments show the growth of computational time is slower than linear growth with respect to search range; 3) the efficiency is less influenced by subset size; as subset size increases from 21 to 63, the average computational time at each POI increases from 0.11 to 0.15 ms; 4) it is easy to select the initial threshold th0; both numerical and real experiments show that the variation of computational time is smaller than 0.1 ms as th_0 increases from 0.5 to 6.0; the selection of the threshold has less influence on the efficiency.

Acknowledgments

The author is grateful to Dr. Zhenyu Jiang (South China University of Technology) for discussions and DIC community for providing high-quality, open-access DIC dataset.

Reference

1. Pan B, Qian K, Xie H et al., "Two-dimensional digital image correlation for in-plane displacement and strain measurement: a review," *Meas. Sci. Technol.* **20**(6), 062001 (2009)
2. Chen DJ, Chiang FP, Tan YS, Don HS, "Digital speckle-displacement measurement using a complex spectrum method," *Appl. Opt.* **32**, 1839–1849 (1993)
3. Zhou P. "Subpixel displacement and deformation gradient measurement using digital image/speckle correlation (DISC)," *Opt. Eng*. **40**, 1613–1620 (2001)

4. Zhang J, Jin G, Ma S, Meng L, “Application of an improved sub-pixel registration algorithm on digital speckle correlation measurement,” *Opt. Laser Technol.* **35**, 533–542 (2003)
5. Bruck HA, McNeill SR, Sutton MA, Peters WH, “Digital image correlation using Newton–Raphson method of partial differential correction,” *Exp. Mech.* **29**, 261–267 (1989)
6. Vendroux G, Knauss WG, “Submicron deformation field measurements: Part 2. Improved digital image correlation,” *Exp. Mech.* **38**, 86–92 (1998)
7. Yuan Y, Huang J, Fang J, et al, “A self-adaptive sampling digital image correlation algorithm for accurate displacement measurement,” *Opt. Lasers Eng.* **65**, 57–63 (2015)
8. Huang J, Pan X, Peng X, et al, “Digital Image Correlation with Self-Adaptive Gaussian Windows,” *Exp. Mech.* **53**(3), 505–512 (2013)
9. Wittevrongel L, Lava P, Lomov SV, Debruyne D, “A self-adaptive global digital image correlation algorithm,” *Exp. Mech.* **55**, 361–378 (2015)
10. Zhou Y, Pan B, Chen Y Q, “Large deformation measurement using digital image correlation: a fully automated approach,” *Appl. Opt.* **51**(31), 7674–7683 (2012)
11. Poissant J, Barthelat F, “A Novel “Subset Splitting” Procedure for Digital Image Correlation on Discontinuous Displacement Fields,” *Exp. Mech.* **50**(3), 353–364 (2010)
12. Valle V, Hedan S, Cosenza P, et al, “Digital Image Correlation Development for the Study of Materials Including Multiple Crossing Cracks,” *Exp. Mech.* **55**(2), 379–391 (2015)
13. Poncelet M, Leclerc H, “A Digital Image Correlation Algorithm with Light Reflection Compensation,” *Exp. Mech.* **55**(7), 1317–1327 (2015)
14. Xu J, Moussawi A, Gras R, et al, “Using Image Gradients to Improve Robustness of Digital Image Correlation to Non-uniform Illumination: Effects of Weighting and Normalization Choices,” *Exp. Mech.* **55**(5), 963–979 (2015)
15. Pan, B., Li, K. and Tong, W, “Fast, robust and accurate digital image correlation calculation without redundant computations,” *Exp. Mech.* **53**(7), 1277–1289 (2013)

16. Pan B, Tian L, “Superfast robust digital image correlation analysis with parallel computing,” *Opt. Eng.* **54**(3), 034106 (2015)
17. Zhang L, Wang T, Jiang Z, et al, “High accuracy digital image correlation powered by GPU-based parallel computing,” *Opt. Lasers Eng.* **69**, 7–12 (2015)
18. Jiang Z, Qian K, Miao H, et al, “Path-independent digital image correlation with high accuracy, speed and robustness,” *Opt. Lasers Eng.* **65**, 93–102 (2015)
19. Pan B, “Reliability-guided digital image correlation for image deformation measurement,” *Appl. Opt.* **48**(8), 1535–1542 (2009)
20. Wu R, Kong C, Li K, et al, “Real-Time Digital Image Correlation for Dynamic Strain Measurement,” *Exp. Mech.* **56**(5), 833–843 (2016)
21. Tombari F, Mattoccia S, Stefano L D, et al, “Full-Search-Equivalent Pattern Matching with Incremental Dissimilarity Approximations,” *IEEE Trans. Pattern Anal. Mach. Intell.* **31**(1), 129–141 (2009)
22. M. McDonnel, “Box-Filtering Techniques,” *Comput. Graph. Image Proc.* **17**, 65–70 (1981)
23. Stark J A, “Adaptive image contrast enhancement using generalizations of histogram equalization,” *IEEE Trans. Image Proc.* **9**(5), 889-896 (2000)
24. https://sem.org/dic-challenge/.

Caption List

Fig. 1 The flow chart of the newly proposed A-IDA algorithm

Fig. 2 Reference image and ROI

Fig. 3 Mean bias and standard deviation error of rigid body translation experiments; subset size 33, $th_0 = 1$, search range in y-axis [-5, 45]

Fig. 4 Reference image and the ROI

Fig. 5 Displacement fields in x-axis and y-axis

Table 1 Average computational time at each POI with respect to pre-set displacement using A-IDA and IC-GN algorithm; subset size 33 × 33 pixels, th_0 = 1, search range in y-axis [-5, 45]

Table 2 Average computational time at each POI with respect to search range; pre-set displacement 10.50 pixels, subset size 33 × 33 pixels, th_0 = 1

Table 3 Average computational time at each POI with respect to subset size; pre-set displacement 10.50 pixels, th_0 = 1, search range in y-axis [-5, 45]

Table 4 Average computational time at each POI with respect to initial threshold; pre-set displacement 10.50 pixels, subset size 33 × 33 pixels, search range in y-axis [-5, 45]

Table 5 Average computational time with respect to th_0 at each POI using A-IDA and IC-GN algorithm in the real experiments; subset size is 33 × 33 pixels with p = 3 and the search ranges are [-20, +20] and [-5, +5] in x-axis and y-axis, respectively